Methods for the detection and the characterization of low mass companions using the IFS of SPHERE

Zurlo A. [ab], Mesa D. [b], Gratton R. [b], Claudi R. [b], Desidera S. [b],
Giro E. [b], Beuzit J.-L. [c], Dohlen K. [a], Mouillet D. [c], Puget P. [c], Wildi F. [d],
Feldt M. [e], Moeller-Nilsson O.[e], Baruffolo A. [b], Fantinel D.[b], Salasnich B. [b], Kasper M.[f],
Costille A. [a], Sauvage J.-F. [g], Vigan A. [a], Moutou C. [a], Langlois M. [h], Antichi J. [i],
Pavlov A. [e], Zimmerman N.[f], Turatto M.[b]

[a]Aix Marseille Université, CNRS, LAM (Laboratoire d'Astrophysique de Marseille) UMR 7326, 13388, Marseille, France;
[b] INAF-Osservatorio Astronomico di Padova, Vicolo dell'Osservatorio 5, 35122, Padova, Italy;
[c] UJF-Grenoble 1 / CNRS-INSU, Institut de Planétologie et d'Astrophysique de Grenoble (IPAG) UMR 5274, Grenoble, F-38041, France;
[d] Observatoire de Genéve, University of Geneva, 51 Chemin des Maillettes, 1290, Versoix, Switzerland;
[e] Max-Planck-Institut für Astronomie, Königstuhl 17, 69117 Heidelberg, Germany;
[f] European Southern Observatory, Karl-Schwarzschild-Strasse 2, D-85748 Garching, Germany;
[g] ONERA - The French Aerospace Lab BP72 - 29 avenue de la Division Leclerc FR-92322 CHATILLON CEDEX;
[h] CRAL, UMR 5574, CNRS, Université Lyon 1, 9 avenue Charles André, 69561 Saint Genis Laval Cedex, France;
[i]INAF - Osservatorio Astrofisico di Arcetri - L.go E. Fermi 5, I-50125 Firenze, Italy

ABSTRACT

SPHERE is an instrument aimed to the search for low mass companions around young stars in the solar neighborhood. To achieve this goal light from the host star (and in particular the speckle pattern due to the telescope aberrations) should be strongly attenuated while avoiding to cancel out the light from the faint companion. Different techniques can be used to fulfill this aim exploiting the multi-wavelength datacube produced by the Integral Field Spectrograph that is one of the scientific modules that composes SPHERE. In particular we have tested the application of the Spectral Deconvolution and of the Principal Components Analysis techniques. Both of them allow us to obtained a contrast better than 10^{-5} with respect to the central star at separations of the order of 0.4 arcsec. A further improvement of one order of magnitude can be obtained by combining one of these techniques to the Angular Differential Imaging. To investigate the expected performance of IFS in characterizing detected objects we injected in laboratory data synthetics planets with different intrinsic fluxes and projected separations from the host star. We performed a complete astrometric and photometric analysis of these images to evaluate the expected errors on these measurements, the spectral fidelity and the differences between the reduction methods. The main issue is to avoid the strong self-cancellation that is inherent to all the reduction methods. We have in particular tested two possible solutions: the use of a mask during the reduction on the positions of the companions or, alternatively, using a KLIP procedure for the IFS. This latter seems to give better results in respect to the classical PCA, allowing us to obtain a good spectral reconstruction for simulated objects down to a contrast of $\sim 10^{-5}$.

Keywords: Spectrograph, planetary systems, direct imaging, high angular resolution

1. INTRODUCTION

Until now just 47 extrasolar planets out of more than 1700 have been discovered exploiting the direct imaging technique. This is mainly due to the very high luminosity contrast (of the order of $\sim 10^{-6}$ for a young giant planets and of the order of $10^{-8} - 10^{-9}$ for a old giant or rocky planet shining mostly through reflected light) and the very small separation (of the order of few tenths of arcsec for planets orbiting at ~10 AU stars at distance up to tens of parsecs from the Sun) from

Ground-based and Airborne Instrumentation for Astronomy V, edited by
Suzanne K. Ramsay, Ian S. McLean, Hideki Takami, Proc. of SPIE Vol. 9147,
914770 · © 2014 SPIE · CCC code: 0277-786X/14/$18 · doi: 10.1117/12.2055085

their host star. The number of imaged extrasolar planets is however going to greatly increase after that a new generation of instruments devoted to implement this technique is going to become operative. The most important of these instruments are the Gemini Planet Imager (GPI[1]) now operating at the Gemini South Telescope and SPHERE (Spectro-Polarimetric High-contrast Exo-planet REsearch[2]) that is in this period in its commissioning phase at the ESO Very Large Telescope (VLT).

SPHERE is composed by four subsystems:

- an Extreme Adaptive Optics (ExAO) system called SAXO[3] that produces a highly stabilized beam with a Strehl Ratio (SR) of more than 90%;
- the Common Path and Infrastructure (CPI) that brings the telescope light to the three scientific modules. The CPI contains the deformable mirror (DM), relay optics such as torric mirrors,[4] derotator, atmospheric dispersion compensators and coronagraphs;
- the Zurich IMager POLarimeter, ZIMPOL[5] operating in the visible between 500 and 900 nm and exploiting the polarization of the light reflected by the atmosphere of the planets to perform differential imaging;
- the Infra-Red Dual-beam Imager and Spectrograph, IRDIS[6] is an infrared dual-band imager and a spectrograph that can operate exploiting various observing modes: classical imaging (CI), dual-band imaging (DBI[7]), polarimetric imaging (DPI[8]) or long-slit spectroscopy (LSS[9]). It works in the near infrared between 0.95 and 2.32 μm with a field of view (FOV) of 12.5×11 arcsec;[6]
- the Integral Field Spectrograph, IFS[10] operating in the near infrared between 0.95 and 1.35 μm with a spectral resolution of 50 when in the YJ-mode and between 0.95 and 1.65 μm with a spectral resolution of 30 when in the YH-mode.

In this paper we will describe the laboratory tests that have been performed on the IFS at the Institute de Planétologie et d'Astrophysique de Grenoble (IPAG), the technique that we have developed to subtract the speckle pattern from these data and the results that we have obtained concerning the contrast that can be obtained with the instrument. Moreover, we will present the foreseen performance for the instrument regarding astrometry and photometry of the found companion objects obtained injecting simulated planets into the laboratory data.

2. IFS TEST IN LABORATORY

The data were acquired during the Assembly Integration and Testing (AIT) phase while the instrument were at the IPAG. During the period of the tests, between the end of 2011 and the end of 2013, a telescope simulator (TSIM) was mounted in front to the instrument to have a realistic pupil similar to the one of the VLT.

On the same simulator a phase screen was mounted with the aim to simulate atmospheric turbulence to recreate conditions similar of Paranal. The possible values of the seeing that can be simulated are 0.6, 0.8 and 1.2 arcsec and a wind speed ranging from 2 to 10 m/s.

The data for the SPHERE instrument are taken exploiting the instrument control software (INS). INS is divided in different components called templates that perform particular tasks that can be performing all the requested calibration or running the scientific observations.[11] All the data taken in this way are then reduced exploiting the Data Reduction and Handling (DRH) software[12] that is composed in different procedures (called recipes) that are aimed to reduce the data coming from each INS template. The most important calibrations to be performed before of each scientific observation run is the following:

- dark frames,
- detector flat,
- definition of the position of each spectrum on the detector,
- wavelength calibration for each spectrum,

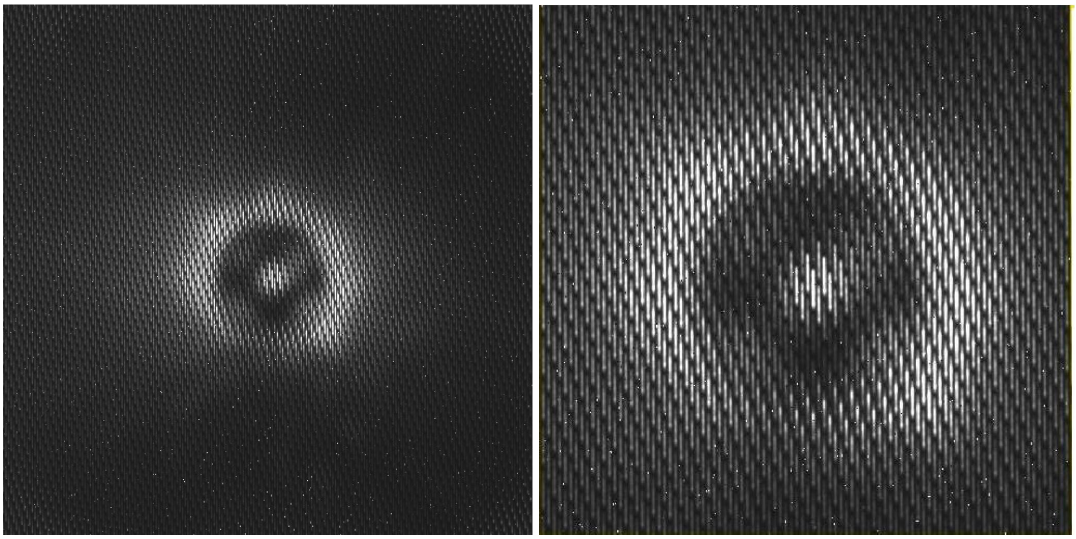

Figure 1. *Left*: Example of scientific image obtained during the IFS tests. *Right*: Zoom of the central part of the scientific image.

- instrument (or IFU) flat that is used to take account of the different response from different lenslets of the IFU array to a uniform illumination.

The science data can be acquired through three different templates. One of them is used for observations in YJ-mode, the second one is used for observations in the YH-mode while the third one is used to perform survey at the near infrared wavelengths. All the IFS observations are performed in parallel with IRDIS that is used for acquisition purposes like coronagraphic fine centering. SPHERE allows to use different types of coronagraphs as three apodized Lyot coronagraphs with different mask diameters optimized for observations at different wavelengths, and two four quadrant coronagraphs. All of them have been tested during the tests but in this work we will present just the results obtained using the apodized Lyot coronograph with the mask diameter of 185 mm. Moreover, in the following Sections we will present results obtained simulating a star with J=2.6, with a seeing of 0.8 arcsec and a wind speed of 5 m/s (typical conditions for Paranal). A typical scientific image obtained during the IFS test is shown in Figure 1 (left) while a zoom of the central part of the same image is shown in Figure 1 (right) to enlighten the structure of the spectra.

3. DATA REDUCTION

The data reduction is performed exploiting the DRH recipes until to the building of the final science datacube that is composed by 39 monochromatic images with dimension of 291×291 pixels. On this datacube we have performed data reduction procedures written in IDL aimed to subtract the speckle pattern. To minimize calibration errors we prepared a procedure to define precisely the position of the center of the star and to define the rescaling factor to be applied to each monochromatic image. At this aim we took images with the presence of waffles. The waffles are 4 replies of the central PSF put in symmetrical positions with respect to the central star. They are introduced by SAXO in closed-loop operations, modifying in an appropriate way the AO reference slopes. Their symmetric positions with respect to the center of the star can be exploited to define the position of the star center. Moreover, as these spots, like the speckle pattern, change their distance from the star center according to the wavelength, their positions in images at different wavelengths can be exploited to define the rescaling factor for each monochromatic image in the datacube.

On this registered datacube is then possible to apply the speckle pattern subtraction procedures. For our data we have implemented the Spectral Deconvolution[13,14] (SD) and the Principal Components Analysis[15] (PCA). Our implementation of these two methods is described in Section 3.1, 3.2, 3.3. A more detailed description of these method can be found in Mesa et al. (submitted) and Zurlo et al. (submitted).

3.1 Spectral Deconvolution

A schematic description of the SD is the following:

- each monochromatic image is rescaled in such a way that the speckle pattern is very similar for each wavelength while the companion is in different positions,
- a polynomial fit is performed along the wavelength direction for each pixel of the rescaled datacube,
- the fit is subtracted from the rescaled datacube to reduced the speckle noise,
- each monochroamtic image is rescaled back to its original position in such a way that the companion position is the same in each image.

The registering described above allows us to have a very well aligned datacube but we have still to deal with some problems. One of these problems is the fact that the image is not uniformly illuminated probably because the presence of a ghost into the telescope simulator optics. To deal with this problem we have subtracted from each monochromatic image a bi-dimensional fit of the image itself. Moreover, we noted that even after the rescaling, the full width at half maximum (FWHM) of the waffles has not the same dimensions and this can result in a not perfect subtraction of the speckles pattern. To solve this problem we have slightly smoothed each monochroamtic images in such a way that the speckles FWHM is the same for all the wavelengths. Finally, we have performed a normalization of the flux of the images at different wavelengths dividing them in 8 radial sectors. The normalization factors have been calculated considering the flux of the images at separations form the star center ranging between 6 and 15 λ/D.

After all this preparatory work, we were able to implement our IDL version of the SD. To make the procedure more effective and avoid the subtraction of the planetary signal, we excluded from the spectrum to be fitted all the pixels around the maximum of the spectrum if larger than its median plus fifteen times the standard deviation of the remaining part of the spectrum itself. The number of excluded pixels is calculated accordingly to the fraction of the spectrum that would be covered by a possible planet at the separation under consideration according to Ref 14.

In Figure 2 we display the 5σ contrast plot that we obtain applying the SD to our data. The blue dashed line represents the contrast that we obtained without taking into account the cancellation effects that are caused on the companion objects by all the speckle subtraction methods using just one datacube. The blue solid line is the contrast that we obtain after that the cancellation effects are properly taken into account. The red and orange lines are obtained subtracting each other datacubes taken in different times with the aim to simulate the Angular Differential Imaging[16] (ADI). In this latter case the final contrast that we obtain is better of one order of magnitude than the contrast obtained without using it.

3.2 Principal Component Analysis

The preparation of the datacube for the application of the PCA procedure is similar to the one described in Section 3.1. The only difference that we avoid to divide the image in different sectors when calculating the normalization factor. The following step consists in the subtraction of a stellar profile from each image of the datacube. We then use the central part of each image composed by 200×200 pixels centered on the center of the star to fill the two-dimensional array that is used as input of the PCA procedure. The PCA is implemented exploiting the singular value decomposition algorithm which generates three arrays that, combined in the correct way, lead to the eigenvectors and the eigenvalues used to reconstruct the original data. The principal components for this reconstruction are given by the matrix product of these two arrays. A principal components subset is used to generate an image containing the quasi-static noise pattern that can then be subtracted from the original image. The larger the number of the principal components, the better the noise subtraction, but, on the other hand, this could produce strong cancellation of a faint companion.

In Figure 3 we display the final 5σ contrast that we obtain applying the PCA. As for the SD case, the dashed blue line is obtained applying the PCA to a single datacube without taking into account the cancellation effects, while the solid blue line is obtained taking them properly into account. The red line is the contrast that we can obtain using a larger number of datacube and for this reason it is possible to use a larger number of principal components.

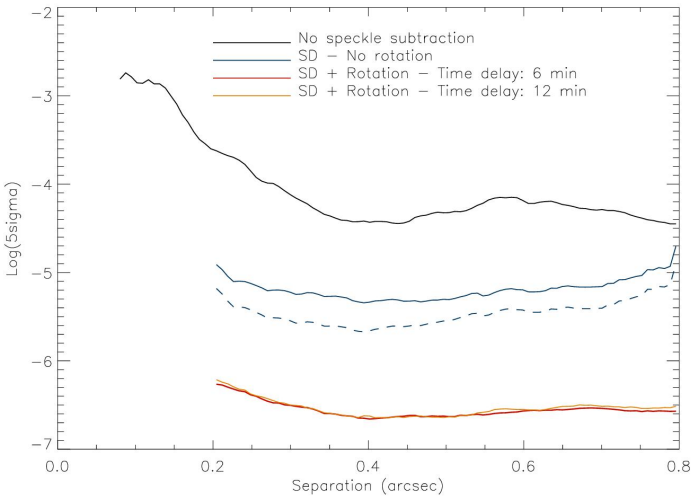

Figure 2. 5σ contrast plot obtained applying the SD method.

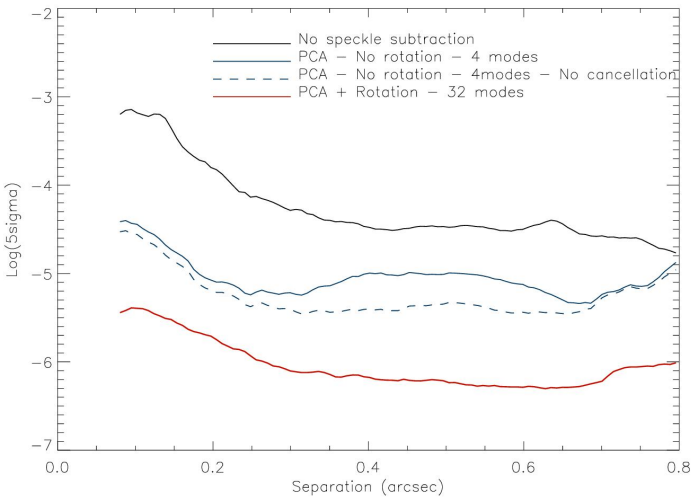

Figure 3. 5σ contrast plot obtained applying the PCA method.

3.3 KLIP

More suitable for the characterization of the companions that will be detected by IFS, we implemented a PCA method that performs the KLIP (Karhunen–Loève Image Projection) algorithm, following the model of Ref15 with improvements dedicated to the spectral extraction from IFS datacubes developed for Project 1640 data (Pueyo et al., submitted).

This method will reduce the cancellation induced by the other reduction method listed so far and for this reason it will be used especially for the characterization after the detection of a candidate.

KLIP takes advantage of the multiple channels of the IFS to create the reference library for the basis of the Karhunen–Loève matrix. The signal of the planet after the spatial rescaling of the IFS datacube is in different positions with respect to the center of the image while the speckles pattern remains fixed. If we take as a reference a small portion of one monochromatic image around the position of the planet, it is possible to create a reference library using a characterization zone that is included in the projection of this portion on all the other channels that contain no signal from the planetary candidate, or at least or a very small quantity of it.

We used the forward modeling method presented in Ref15 to get our results in KLIP photometry, as we will show in Sect. 4.1. On-sky observations are expected to produce even better results, as the construction of the PCA library will exploit also the FoV rotation.

4. SYNTHETIC PLANETS SIMULATIONS

To estimate the errors on the photometry and astrometry of the future candidates, we injected synthetic planets on the set of data presented in Sec. 3. The latter was taken in parallel with IRDIS subsystem, but in this paper we will present the analysis concerning IFS and we refer the reader to Zurlo et al. (submitted) for the detailed complete analysis.

The synthetic planets consist of a small portion of the off-axis PSF acquired during the scientific sequence to take into account the second ring of diffraction and the light diffracted by the spiders. The synthetic companions have been introduced in the scientific datacube before SD or KLIP analysis.

The flux of the PSF has been rescaled to reproduce L and T-type spectra. The libraries of field brown dwarfs used for the L-type spectra are taken from Ref 17, while the T-type ones are from Ref 18, Ref 19 and Ref 20.

Five simulated planets were injected simultaneously at five different separations (0.20, 0.35, 0.50, 0.65, 0.80 arcsec) and position angles with respect to the star. To improve the statistical significance of the results, the procedure was repeated 30 times with position angles shifted by steps of 12 degrees each time. The flux of the planets was scaled for five different contrast levels (10^{-3}, $3{\times}10^{-4}$, 10^{-4}, $3{\times}10^{-5}$ and 10^{-5}) with respect to the host star. The contrast was defined as the ratio between the integrated flux of the planet over that of the star, over the whole band covered by IFS and IRDIS (0.8–1.8 μm). Overall, the statistic of our results is based on a total of 750 injected planets (5 planets each image, 5 contrasts, 30 different rotation angles) of the same spectral type.

An example of the simulated planet inserted in the scientific datacube and after SD reduction is also shown in Fig. 4.

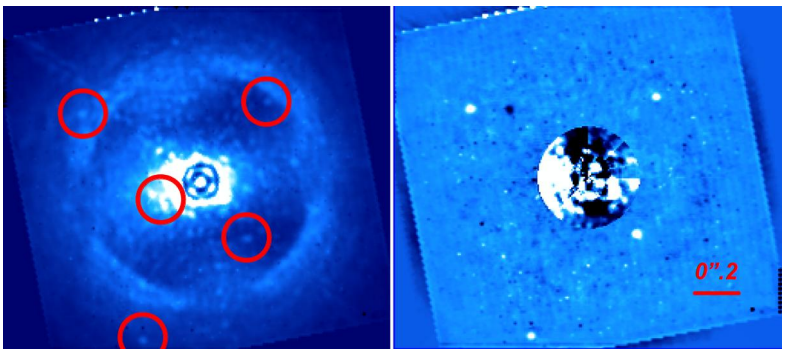

Figure 4. Simulated T5-type planets at a contrast of 3×10^{-5} injected in the IFS pre-reduced datacube (left) and after the SD reduction (right). In the central part of the image an optimization has been tuned to improve speckles subtraction. The images show the 15th channel of IFS at $\lambda = 1.09\ \mu$m.

4.1 Results on photometry

To estimate the errors on the photometry measurements with IFS after SD and KLIP reductions we performed PSF-fitting photometry on the data where we injected planets. The two reductions methods have been analyzed separately. The positions of the companions are assumed to be known.

We retrieved a model of the off-axis PSF using a Moffat function for each spectral channel and comparing it with the PSFs of the planets. The contrast is calculated pixel by pixel after alignment of the centers of the PSFs of the star and the planet. The final result is calculated as the weighted median of all the pixels inside a radius of $1.2\lambda/D$. The same procedure was performed using a 2-d Moffat function that reconstructs exactly the off-axis PSF of the star, obtaining the same results.

A special version of the SD routine has been implemented with the purpose of minimize the flux loss. This routine applies a mask to protect the planet around its position during the reduction. In order to improve KLIP results we used an implementation of the forward modeling presented in Ref 15. The final errors on photometry for each channel of IFS are the standard deviation of the residuals of all the planets with the same separation, flux and wavelength.

To evaluate which method is best to use as a function of separation and contrast, we calculated the standard deviation of the photometry offsets obtained reducing the data with the SD and KLIP techniques. The results of this analysis are presented in Fig. 5. From this evaluation we determined that in general KLIP works better for brighter objects and that its results are comparable with the ones of the SD. Nevertheless we expect that KLIP will greatly improve with the addition of the ADI, that permits to expand the part of the library without signal from the object itself.

Examples of the extracted spectra for T5-type planets at contrasts of 10^{-4} and 10^{-5} and different separations are shown in Fig. 6, with error bars reflecting the dispersion of the results obtained with synthetic planets at different positions within the image. The two IRDIS photometric measurements are represented, too.

4.2 Results on astrometry

For astrometric measurements we used a Levenberg-Marquardt least squares fit, using the IDL routine *mpfit*[21] to calculate the position of the simulated planets on the median of all the IFS spectral channels. We implemented a routine which uses a model of the planets PSFs and tries to cancel the flux of the planet at each iteration, shifting the position of the model around the position of the companion. This means that the flux of the planets is already known and the fit only performs the optimization of the position of each PSF. The fit stops when it finds the minimum value of the standard deviation in a $1.5\lambda/D$ aperture around the position of the planet.

We performed astrometric measurements both on SD and KLIP reduced datacubes. The expected error is calculated taking into account the dependency of the standard deviation of the offsets on the S/N of the candidates. The total numbers of detected planets (S/N > 5) are 523 and 441 out of 600, respectively for the SD (with mask) and KLIP reductions. Planets with separation of 0.20 arcsec are not considered in this analysis because of the very low number of detected planets at this separation. We found that the trend of the standard deviation σ could be described by the following formulas for the SD and KLIP methods, respectively:

$$\sigma_{SD} = 0.15 + \frac{15.64}{S/N}\ mas \tag{1}$$

and

$$\sigma_{KLIP} = 0.05 + \frac{12.25}{S/N}\ mas. \tag{2}$$

We consider that trends reprensent the error on our relative astrometric measurements with IFS. We represent the astrometric offsets along the two cartesian coordinates for the SD analysis in Fig. 7, and for the KLIP analysis in Fig. 8. The respective trend curves defined by Eq. 1 and Eq. 2 is also overplotted.

We can then predict that for a faint planet, with a contrast of 10^{-5}, the typical relative position error will be of the order of 2 mas at a separation of 0.35 arcsec from the host star, while for a brighter planet with a contrast of $3{\times}10^{-4}$ will be of the order of 0.5 mas at the same separation. As discussed in the next Section, these results are comparable and even better to those obtained nowadays exploiting the ADI, even if they are obtained with the only use of SDI techniques.

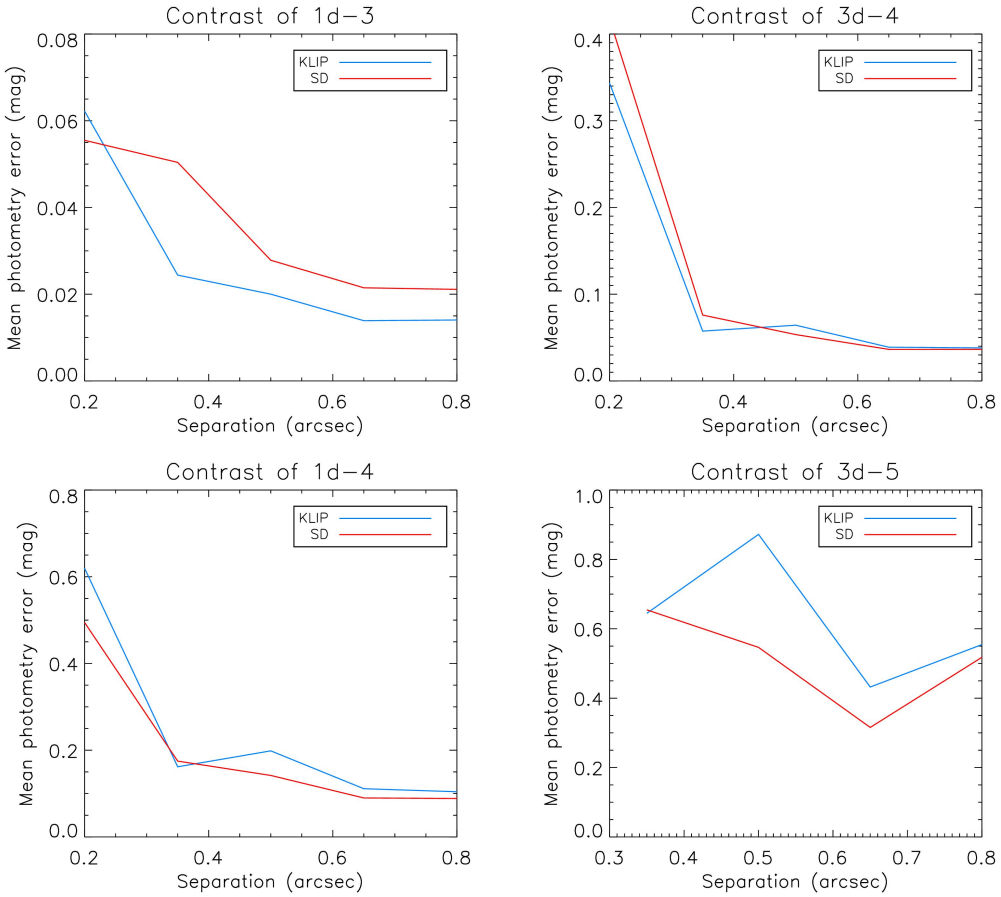

Figure 5. Plots of the expected photometric errors for different contrasts as a function of separation from the central star. Results obtained with KLIP (red line) and SD (blue line) are compared. Each point represents the median of the errorbar on the 39 IFS channels. Only detected planets are considered in this analysis. Very few planets with contrast of 10^{-5} are detected so the corresponding plot is not shown.

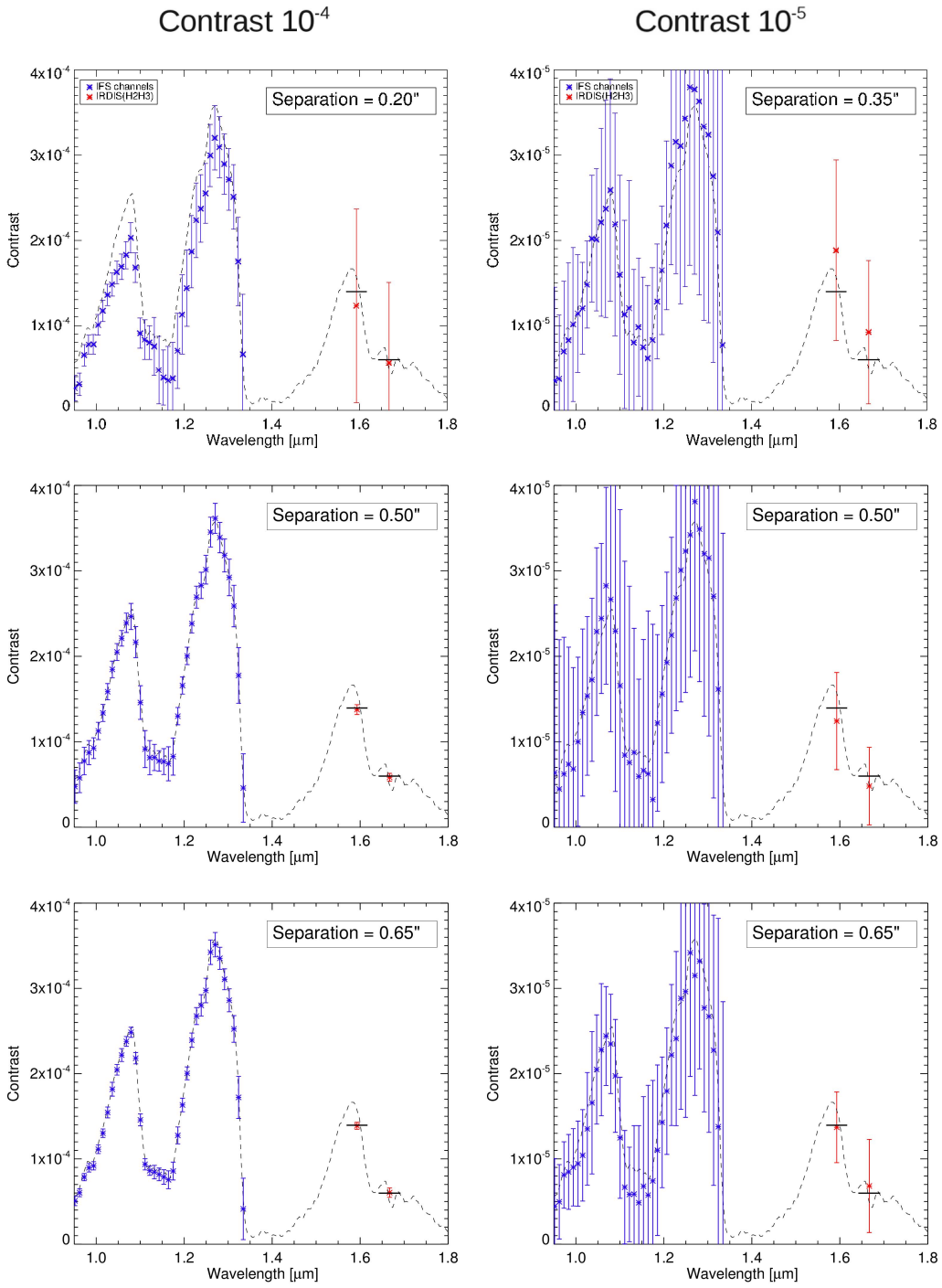

Figure 6. Spectral extraction of a T5 model spectrum (black line) for planets at different separations (from top to bottom) and contrast from the star (10^{-4} on the left, 10^{-5} on the right). The blue points represent the IFS photometry for each channel (reduced with the SD technique), while the red ones represent the flux measurement in the two IRDIS filters *H*2 and *H*3. For IRDIS data, the black horizontal line represent the therotical value of the photometry; each line covers the bandpass of the filters.

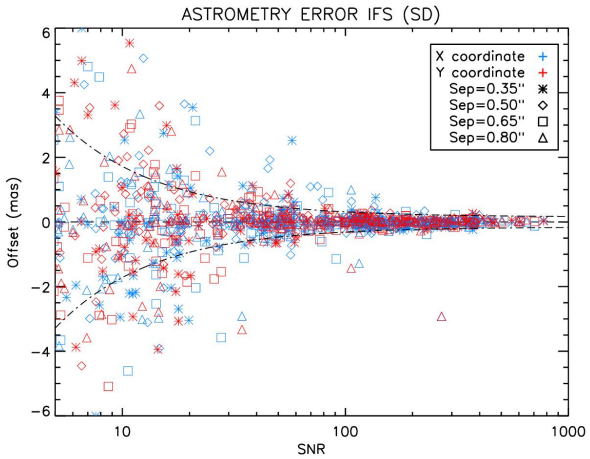

Figure 7. Plot of the difference between nominal and measured astrometric values for the two coordinates versus the S/N of each planet with contrasts from 10^{-5} to 10^{-3} and separations from 0.35 to 0.80 arcsec in the IFS datacube after SD reduction. The dashed black line represents Eq. 1. Different separations from the host star are represented with different symbols.

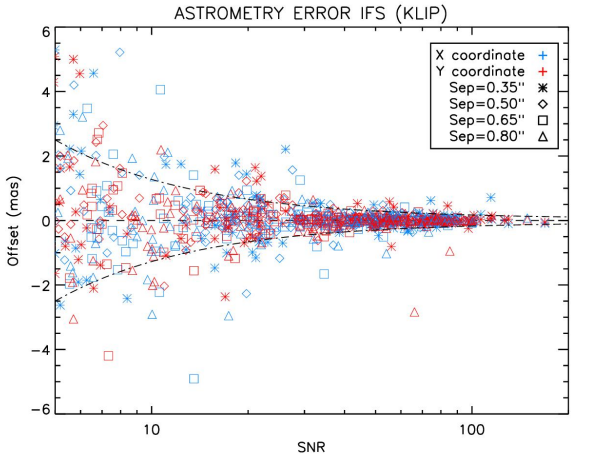

Figure 8. Plot of the difference between nominal and measured astrometric values for the two coordinates versus the S/N of each planet with contrasts from 10^{-5} to 10^{-3} and separations from 0.35 to 0.80 arcsec in the IFS datacube after KLIP reduction. The dashed black line represents Eq. 2. Different separations from the host star are represented with different symbols.

5. CONCLUSION

In this paper we have presented the results of the laboratory tests performed on the SPHERE IFS instrument. During all this period we have developed new and more efficient procedures to reduce the speckle pattern in the scientific datacube obtained applying the DRH software recipes to the IFS raw data. We have shown that the application of our procedures for the SD or for the PCA to a single datacube can allow to obtain a contrast better than 10^{-5}. The combination of more than one datacube in such a way to simulate the ADI procedure (actually no rotation of the FOV was presented in our data) allows to reach a contrast better than 10^{-6} that is the scientific goal of the instrument.

To test the capabilities of the instrument in performing photometry and astrometry we have injected in the raw data a number of simulated planets with different contrasts and separations with respect to the central star. The spectral type of the synthetic objects simulates L and T-dwarfs. We found that the photometric error can vary from a value of 0.02 mag for the brightest objects to a value of 0.6 mag for contrast of the order of 3×10^{-5}. The value of the astrometric error can vary from a value of 0.1 mas for the brightest planets to values of 2.5 mas for the faintest ones. Even considering that in the evaluation of these errors we have not taken into account the platescale uncertainties these results show a very good improvement with respect to instruments of the previous generation.

ACKNOWLEDGMENTS

We are grateful with the SPHERE team and all the people always available during the tests at IPAG in Grenoble. A.Z., D.M., and S.D. acknowledge partial support from PRIN INAF 2010 "Planetary systems at young ages". We acknowledge support from the French National Research Agency (ANR) through the GUEPARD project grant ANR10-BLANC0504-01. SPHERE is an instrument designed and built by a consortium consisting of IPAG, MPIA, LAM, LESIA, Laboratoire Fizeau, INAF, Observatoire de Genève, ETH, NOVA, ONERA, and ASTRON in collaboration with ESO.

REFERENCES

[1] Macintosh, B., Graham, J., Palmer, D., Doyon, R., Gavel, D., Larkin, J., Oppenheimer, B., Saddlemyer, L., Wallace, J., Bauman, B., Evans, J., Erikson, D., Morzinski, K., Phillion, D., Poyneer, L., Sivaramakrishnan, A., Soummer, R., Thibault, S., and Veran, J.-P., "The gemini planet imager," in [*Society of Photo-Optical Instrumentation Engineers (SPIE) Conference Series*], *Society of Photo-Optical Instrumentation Engineers (SPIE) Conference Series* **6272** (2006).

[2] Beuzit, J.-L., Feldt, M., Dohlen, K., Mouillet, D., Puget, P., Antichi, J., Baruffolo, A., Baudoz, P., Berton, A., Boccaletti, A., Carbillet, M., Charton, J., Claudi, R., Downing, M., Feautrier, P., Fedrigo, E., Fusco, T., Gratton, R., Hubin, N., Kasper, M., Langlois, M., Moutou, C., Mugnier, L., Pragt, J., Rabou, P., Saisse, M., Schmid, H., Stadler, E., Turatto, M., Udry, S., Waters, R., and Wildi, F., "Sphere: A 'planet finder' instrument for the vlt," *The Messenger* **125**, 29 (2006).

[3] Petit, C., Sauvage, J., Sevin, A., Costille, A., Fusco, T., Baudoz, P., Beuzit, J.-L., Buey, T., Charton, J., Dohlen, K., Feautrier, P., Fedrigo, E., Gach, J.-L., Hubin, N., Hugot, E., Kasper, M., Mouillet, D., Perret, D., Puget, P., Sinquin, J.-C., Soenke, C., Suarez, M., and Wildi, F., "The sphere xao system saxo: integration, test, and laboratory performance," in [*Society of Photo-Optical Instrumentation Engineers (SPIE) Conference Series*], *Society of Photo-Optical Instrumentation Engineers (SPIE) Conference Series* **8447** (2012).

[4] Hugot, E., Ferrari, M., Hadi, K. E., Costille, A., Dohlen, K., Rabou, P., Puget, P., and Beuzit, J., "Active optics methods for exoplanet direct imaging. stress polishing of supersmooth aspherics for vlt-sphere planet finder," *A&A* **538**, A139 (2012).

[5] Thalmann, C., Schmid, H., Boccaletti, A., Mouillet, D., Dohlen, K., Roelfsema, R., Carbillet, M., Gisler, D., Beuzit, J.-L., Feldt, M., Gratton, R., Joos, F., Keller, C., Kragt, J., Pragt, J., Puget, P., Rigal, F., Snik, F., Waters, R., and Wildi, F., "Sphere zimpol: overview and performance simulation," in [*Society of Photo-Optical Instrumentation Engineers (SPIE) Conference Series*], *Society of Photo-Optical Instrumentation Engineers (SPIE) Conference Series* **7014** (2008).

[6] Dohlen, K., Langlois, M., Saisse, M., Hill, L., Origne, A., Jacquet, M., Fabron, C., Blanc, J.-C., Llored, M., Carle, M., Moutou, C., Vigan, A., Boccaletti, A., Carbillet, M., Mouillet, D., and Beuzit, J.-L., "The infra-red dual imaging and spectrograph for sphere: design and performance," in [*Society of Photo-Optical Instrumentation Engineers (SPIE) Conference Series*], *Society of Photo-Optical Instrumentation Engineers (SPIE) Conference Series* **7014** (2008).

[7] Vigan, A., Moutou, C., Langlois, M., Allard, F., Boccaletti, A., Carbillet, M., Mouillet, D., and Smith, I., "Photometric characterization of exoplanets using angular and spectral differential imaging," *MNRAS* **407**, 71–82 (2010).

[8] Langlois, M., Dohlen, K., Augereau, J.-C., Mouillet, D., Boccaletti, A., and Schmid, H.-M., "High contrast imaging with irdis near infrared polarimeter," in [*Society of Photo-Optical Instrumentation Engineers (SPIE) Conference Series*], *Society of Photo-Optical Instrumentation Engineers (SPIE) Conference Series* **7735** (2010).

[9] Vigan, A., Langlois, M., Moutou, C., and Dohlen, K., "Exoplanet characterization with long slit spectroscopy," *A&A* **489**, 1345–1354 (2008).

[10] Claudi, R., Turatto, M., Gratton, R., Antichi, J., Bonavita, M., Bruno, P., Cascone, E., Caprio, V. D., Desidera, S., Giro, E., Mesa, D., Scuderi, S., Dohlen, K., Beuzit, J., and Puget, P., "Sphere ifs: the spectro differential imager of the vlt for exoplanets search," in [*Society of Photo-Optical Instrumentation Engineers (SPIE) Conference Series*], *Society of Photo-Optical Instrumentation Engineers (SPIE) Conference Series* **7014** (2008).

[11] Baruffolo, A., Fantinel, D., Gluck, L., Salasnich, B., Zins, G., Steiner, P., Micallef, M., Bruno, P., Popovic, D., Donaldson, R., Fedrigo, E., Kiekebusch, M., Soenke, C., and Valles, M. S., "Sphere instrumentation software: a progress report," in [*Society of Photo-Optical Instrumentation Engineers (SPIE) Conference Series*], *Society of Photo-Optical Instrumentation Engineers (SPIE) Conference Series* **8451** (2012).

[12] Pavlov, A., Möller-Nilsson, O., Feldt, M., Henning, T., Beuzit, J.-L., and Mouillet, D., "Sphere data reduction and handling system: overview, project status, and development," in [*Society of Photo-Optical Instrumentation Engineers (SPIE) Conference Series*], *Society of Photo-Optical Instrumentation Engineers (SPIE) Conference Series* **7019** (2008).

[13] Sparks, W. and Ford, H., "Imaging spectroscopy for extrasolar planet detection," *ApJ* **578**, 543–564 (2002).

[14] Thatte, N., Abuter, R., Tecza, M., Nielsen, E., Clarke, F., and Close, L., "Very high contrast integral field spectroscopy of ab doradus c: 9-mag contrast at 0.2arcsec without a coronagraph using spectral deconvolution," *MNRAS* **378**, 1229–1236 (2007).

[15] Soummer, R., Pueyo, L., and Larkin, J., "Detection and characterization of exoplanets and disks using projections on karhunen-loève eigenimages," *ApJ* **755**, L28 (2012).

[16] Marois, C., Lafrenière, D., Doyon, R., Macintosh, B., and Nadeau, D., "Angular differential imaging: A powerful high-contrast imaging technique," *ApJ* **641**, 556–564 (2006).

[17] Testi, L., D'Antona, F., Ghinassi, F., Licandro, J., Magazzù, A., Maiolino, R., Mannucci, F., Marconi, A., Nagar, N., Natta, A., and Oliva, E., "Nics-tng low-resolution 0.85-2.45 micron spectra of l dwarfs: A near-infrared spectral classification scheme for faint dwarfs," *ApJ* **552**, L147–L150 (2001).

[18] Looper, D., Kirkpatrick, J., and Burgasser, A., "Discovery of 11 new t dwarfs in the two micron all sky survey, including a possible l/t transition binary," *AJ* **134**, 1162–1182 (2007).

[19] Burgasser, A., McElwain, M., Kirkpatrick, J., Cruz, K., Tinney, C., and Reid, I., "The 2mass wide-field t dwarf search. iii. seven new t dwarfs and other cool dwarf discoveries," *AJ* **127**, 2856–2870 (2004).

[20] Burgasser, A., Geballe, T., Leggett, S., Kirkpatrick, J., and Golimowski, D., "A unified near-infrared spectral classification scheme for t dwarfs," *ApJ* **637**, 1067–1093 (2006).

[21] Markwardt, C., "Non-linear least-squares fitting in idl with mpfit," in [*Astronomical Data Analysis Software and Systems XVIII*], Bohlender, D., Durand, D., and Dowler, P., eds., *Astronomical Society of the Pacific Conference Series* **411**, 251 (2009).